Electronic Supplementary Information (ESI)

Wet Chemical Synthesis of Intermetallic Pt_3Zn Nanocrystals via Weak Reduction Reaction Together with UPD Process and Their Excellent Electrocatalytic Performances

Qiaoli Chen, Jiawei Zhang, Yanyan Jia, Zhiyuan Jiang*, Zhaoxiong Xie*, and Lansun Zheng

State Key Laboratory for Physical Chemistry of Solid Surfaces, Department of Chemistry, College of Chemistry and Chemical Engineering, Xiamen University, Xiamen, 361005 (China)

E-mail: zxxie@xmu.edu.cn, zyjiang@xmu.edu.cn

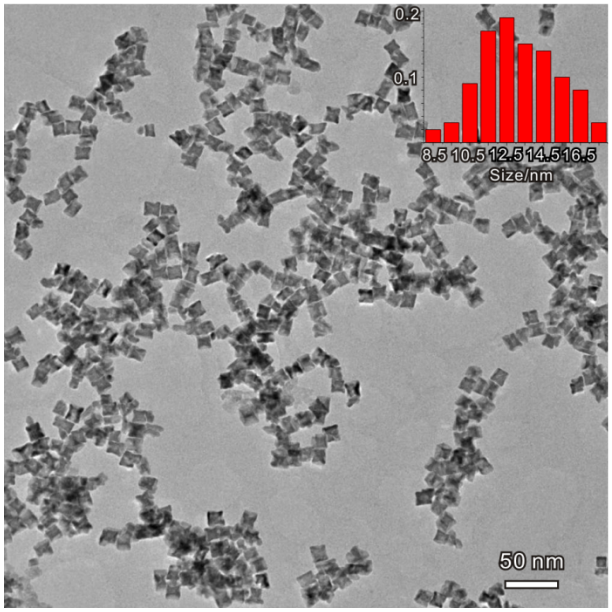

Figure S1. TEM image of the as-synthesized concave cubic intermetallic Pt_3Zn NCs. The insert is the size distribution histogram. The size distribution diagram shows the size of as-synthesized concave cubic intermetallic Pt_3Zn NCs is in the range from 8 nm to 18 nm and with an average value of 12.7 nm.

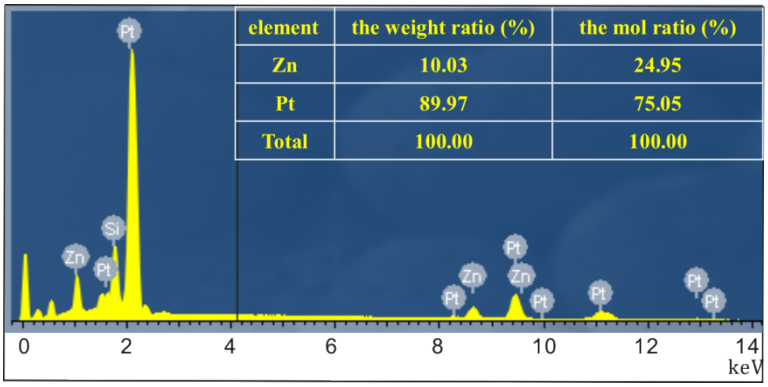

Figure S2. EDS spectrum of the as-synthesized concave cubic intermetallic Pt_3Zn NCs.

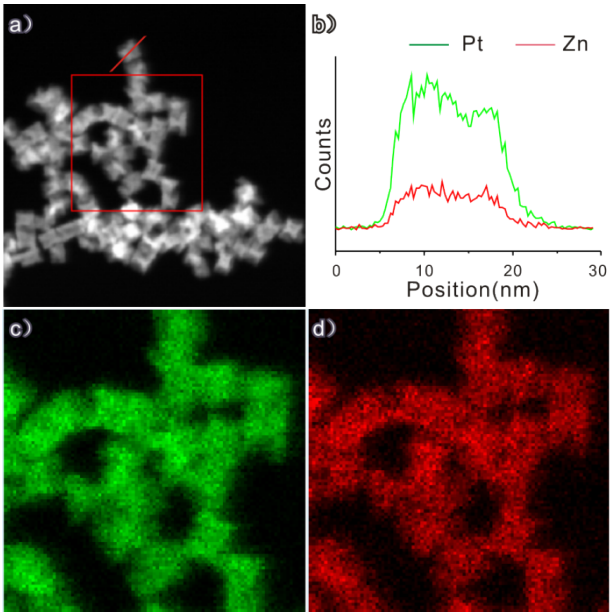

Figure S3. a) HAADF-STEM image of the as-prepared concave cubic intermetallic Pt_3Zn alloy NCs, b) cross-sectional compositional line profile of a single concave cubic intermetallic Pt_3Zn alloy NCs in a), c-d) corresponding elemental map showing the distribution of Pt (green) and Zn (red).

Table S1. Projection angles and geometrical parameters of concave cubic NCs bounded by different high-index facets.

Polyhedral projection direction	Geometrical model of polyhedron	Equations for the projection angles and Miller indices	Calculated projection angles	
<001>	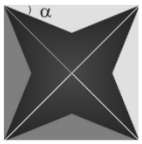	arctan(k/h)	{hk0}	α
			{520}	21.8°
			{730}	23.2°
			{210}	26.6°
			{530}	31.0°
<011>	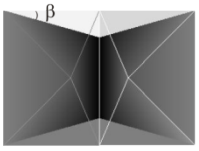	arctan(k/√2h)	{hk0}	β
			{520}	15.8°
			{730}	16.8°
			{210}	19.5°
			{530}	23.0°

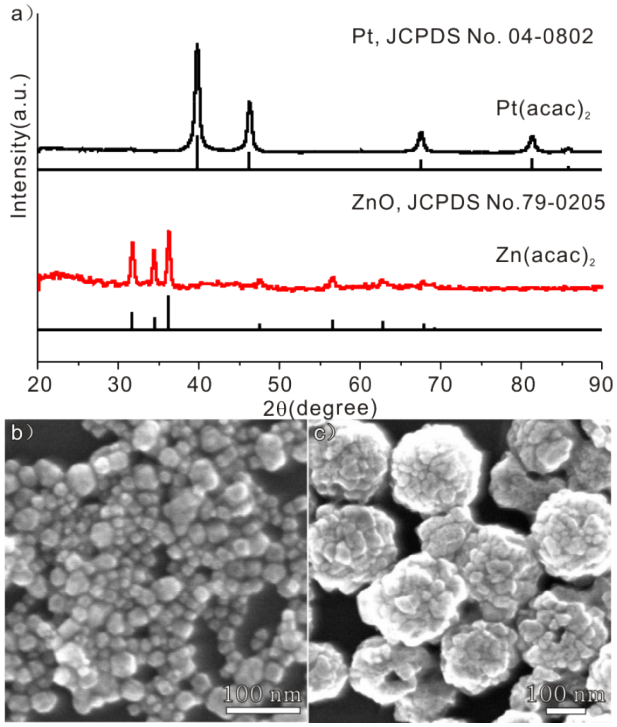

Figure S4. a) XRD patterns of products from precursors $Pt(acac)_2$ and $Zn(acac)_2$, which are metallic Pt and ZnO, respectively; b) SEM image of Pt NCs from $Pt(acac)_2$; c) SEM image of ZnO NCs from $Zn(acac)_2$.

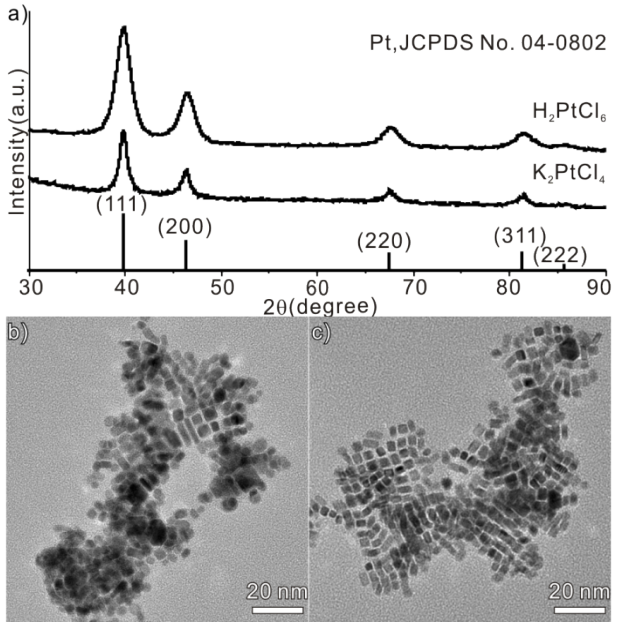

Figure S5. a) XRD patterns of products from $Zn(acac)_2$ and different platinum precursors; b)TEM image of products from $Zn(acac)_2$ and H_2PtCl_6; c) TEM image of products from $Zn(acac)_2$ and K_2PtCl_4.

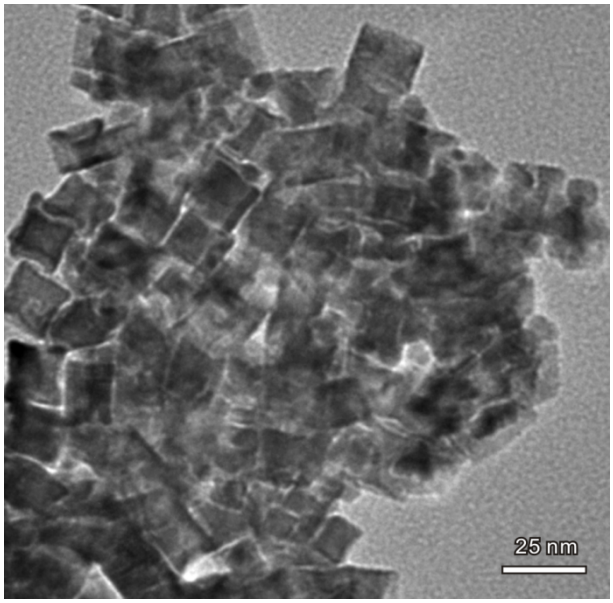

Figure S6. TEM image of products collected from the reaction with the same condition used in the synthesis of concave Pt_3Zn NCs but in the absence of PVP.

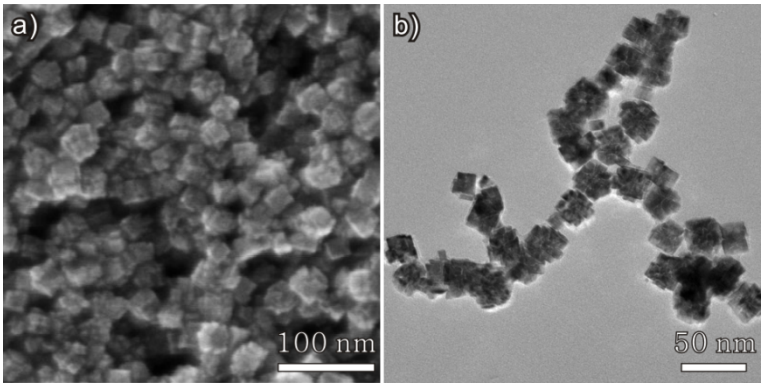

Figure S7. SEM image and TEM image of Pt-Zn alloy NCs.

Table S2. Detailed data about CO stripping obtained from the as-prepared concave cubic intermetallic Pt_3Zn NCs , solid solution Pt_3Zn NCs and the commercial Pt/C.

	Catalysts	E_{onset} / V	$E_{oxidation\ peak}$ / V
CO Stripping	intermetallic Pt_3Zn	0.270	0.465
	solid solution Pt_3Zn	0.341	0.507
	Pt/C	0.462	0.544

Table S3. Detailed data about electrocatalytic oxidation of methanol and formic acid obtained from as-prepared concave cubic intermetallic Pt_3Zn NCs , solid solution Pt_3Zn NCs and the commercial Pt/C.

	Catalysts	j_f / mAcm^{-2}	j_b / mAcm^{-2}	j_f/j_b
Methanol oxidation	intermetallic Pt_3Zn	2.58	1.48	1.74
	solid solution Pt_3Zn	2.19	1.44	1.52
	Pt/C	1.51	1.56	0.97
Formic acid oxidation	intermetallic Pt_3Zn	2.77	4.44	0.62
	solid solution Pt_3Zn	1.35	2.32	0.58
	Pt/C	0.73	3.02	0.23

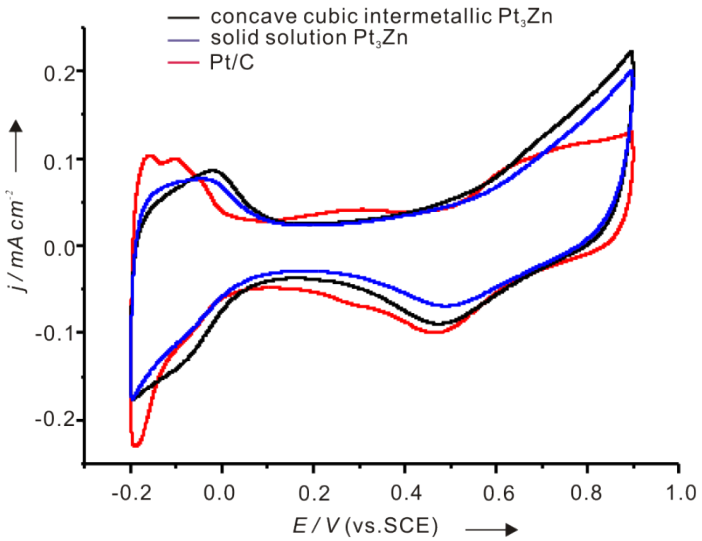

Figure S8. CV curves of concave cubic intermetallic Pt_3Zn alloy NCs, solid solution Pt_3Zn alloy NCs and commercial Pt/C recorded in 0.10 M H_2SO_4 solution. Scan rate: 50 mV s^{-1}.

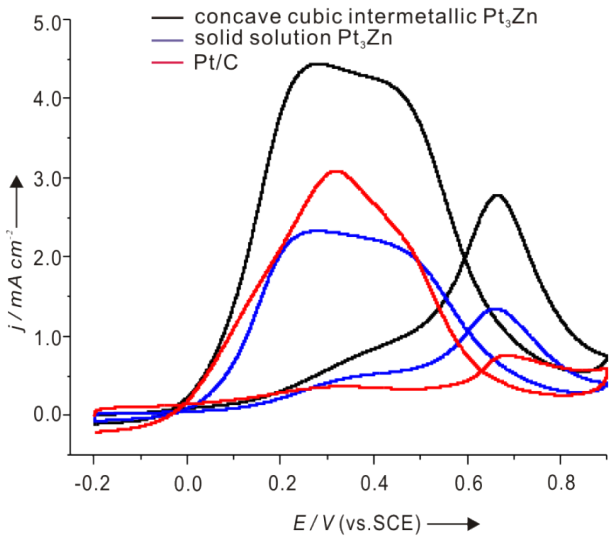

Figure S9. Formic acid oxidation of concave cubic intermetallic Pt_3Zn alloy NCs, solid solution Pt_3Zn alloy NCs and commercial Pt/C in 0.50 M H_2SO_4 + 0.25 M formic acid solution (scan rate: 50 mV s^{-1}).

In order to further demonstrate the excellent electrocatalytic activity arising from outstanding CO removal capacity, the electro-oxidation of formic acid (another common fuel molecule) was also used as a probe to examine the electrocatalytic activity of the as-prepared concave cubic intermetallic Pt_3Zn NC. Figure S8 shows the corresponding CV curves recorded in solution of 0.50 M H_2SO_4 + 0.25 M formic acid at a scan rate of 50 mV s^{-1}. It is well known that the formic acid oxidation can proceed through two parallel ways: one is the direct path, that HCOOH is direct oxidation into CO_2; the other is the indirect path, that HCOOH is converted into adsorbed CO and then to CO_2. In the Figure S8, the peak representing the direct oxidation of formic acid to CO_2 at about 0.4 V of forward scan is obvious, indicating that the process of direct oxidation of formic acid increases with alloying of Zn. In this case, the process of producing CO by formic acid indirect-oxidation is reduced, and thus CO poisoning is decreased. By comparing the j_f/j_b value, that 0.62, 0.58 and 0.23 for the as-prepared concave cubic intermetallic Pt_3Zn NCs, solid solution Pt_3Zn NCs and the commercial Pt/C for the electrooxidation of formic acid, we can also find that the much more improved CO-tolerance capacity of the concave cubic intermetallic Pt_3Zn NCs (Table S3). In addition to the enhanced CO-tolerance, the measured oxidation current densities on the concave cubic intermetallic Pt_3Zn NCs were twice more than that on commercial Pt/C for the formic acid oxidation.